Application of discrete unified gas kinetic scheme to thermally induced nonequilibrium flows

Lianhua Zhu, Zhaoli Guo*

State Key Laboratory of Coal Combustion, School of Energy and Power Engineering, Huazhong University of Science and Technology, Wuhan, 430074, China

Abstract

In this article, we present the applications of the discrete unified gas kinetic scheme (DUGKS) for simulating thermal induced non-equilibrium flows. Four different types of thermally induced flows, including the thermal creep flow, thermal edge flow, radiometric flow and temperature discontinuity induced flow have been simulated in a wide range of Knudsen numbers. The numerical results have been compared with direct simulation Monte Carlo (DSMC) solutions and show that the Shakhov model based DUGKS can be faithfully used for such thermally induced nonequilibrium flows. In particular, due to the asymptotic preserving property of the DUGKS, the flow features in the near continuum flows can be captured efficiently. The extremely low-speed character of such flows is also in favor of the current deterministic model equation solver.

Keywords: Discrete Unified Gas Kinetic Scheme, DSMC, Knudsen force

1. Introduction

Under rarefied conditions, flow of gasses can be induced by the inhomogeneities of temperature fields or the variations of temperature at solid boundaries involved in the system as the characteristic length is comparable to the molecular mean-free-path. Typical examples include thermal creep (or thermal transpiration) flow in a channel as the temperature gradient is applied along the channel walls [1], radiometric flow around a solid plate with different surface temperatures immersed in a vacuum [2], and flow between a heated cantilever next to a cold substrate inside a vacuum enclosure [3]. Although the speed of such temperature-induced nonequilibrium (TINE) flows is usually very low in comparison with sound speed, various potential applications have been identified, such as Knudsen pump [4] and mesosphere flight vehicle [5].

Depending on pressure conditions or device sizes, TINE flows can fall into different flow regimes based on the Knudsen number defined by $\mathrm{Kn} = \lambda/L$ (with λ being the molecular mean-free-path and

*Corresponding author
Email address: zlguo@hust.edu.cn (Zhaoli Guo)

L the characteristic length), i.e., continuum regime (Kn < 0.001), slip regime ($0.001 \leq$ Kn < 0.1), transition regime ($0.1 \leq$ Kn < 10), and free-molecular regime (Kn ≥ 10). It is a challenging problem to develop an efficient numerical method that is applicable to all or multiple flow regimes. The modern computational fluid dynamics (CFD) methods based on the classical continuum theory is not sufficient to describe the dynamics behaviors of such flows beyond the continuum regime, the methods based on extended hydrodynamic models (e.g., Grad's 13 moment, Burnet and super-Burnet equations) also face many theoretical and numerical difficulties although they can be designed for non-equilibrium flows [6]. Therefore, numerical approach based on kinetic descriptions have received wide applications in the study of TINE flows (e.g., Refs. [3, 7–18], among which the stochastic direct simulation Monte-Carlo (DSMC) method and the deterministic discrete ordinates method (DOM) based on kinetic model equations are possible the most popular ones. Due to the extremely low Mach number of typical TINE flows, the DSMC method needs a very long time averaging to lower the statistic noise in the velocity field. Another problem the DSMC method faces is the huge computational cost in simulating near continuum flows as it follows a time-splitting algorithm, namely, the dynamics of a simulated particle is decoupled into free-flight and collision processes, and thus the time step and mesh size are required to be less than the relaxation time and mean-free-path, respectively. It is noted that some improved DSMC algorithms to reduce statistic noises have been developed (e.g., Refs. [19–21]), but the restrictions on time step and mesh size are still not released. The DOM solves the Boltzmann or model equations with discrete velocities and suitable time and space discretizations. A problem in classical DOM is that splitting treatment as DSMC is adopted in the discretization of the kinetic equation, and thus the constraints on time step and grid size still exist [22]. As such, some kinetic schemes with asymptotic preserving (AP) properties have been developed for capturing both continuum and free-molecular flow dynamics in a uniform numerical framework [23–26].

Recently, an AP method, discrete unified gas kinetic scheme (DUGKS), was developed for gas flows ranging from continuum to rarefied regimes [27, 28]. The restriction on time step mesh size is removed in the DUGKS and the finite-volume formulation enables the scheme to handle problems with complex geometries [29]. The DUGKS was already successfully applied to low-speed nearly incompressible flows and high-speed compressible flows ranging from continuum to free-molecular regimes [27–32], but its capability to resolve the low-speed TINE flows has not been tested previously. In this work, we will apply the DUGKS to several typical TINE systems to validate its effectiveness in simulating such non-equilibrium flows.

The remainder of the paper is organized as follows. Section 2 gives a brief introduction of the DUGKS, together with some analysis of its fundamental properties; then numerical simulations of

several types of typical TINE flows (Thermal creep in a closed channel, radiometer flow around a thin plate, flow induced by a hot microbeam immersed in a cavity and flow induced by temperature discontinuities) are carried out in Sec. 3, with some comparisons with the DSMC data; A brief summary is finally given in Sec. 4.

2. Discrete unified gas kinetic scheme

2.1. The Shakhov model equation

The governing equation used in this work is the Shakhov model equation [33] in which the collision term of the original Boltzmann equation is approximated by a relaxation term. In two-dimensional space the Shakhov model equation reads as,

$$\frac{\partial f}{\partial t}+\xi_x\frac{\partial f}{\partial x}+\xi_y\frac{\partial f}{\partial y}=-\frac{1}{\tau}\left[f-f^S\right], \tag{1}$$

where $f=f(\xi_x,\xi_y,\eta,x,y,t)$ is the velocity distribution function of particles with velocity $\boldsymbol{\xi}=(\xi_x,\xi_y)$ in the x- and y-directions, and velocity η in the z-direction at position (x,y) at time t. In Eq. (1), τ is the relaxation time (mean collision time) and is related to the pressure p and gas viscosity μ by $\tau=\mu/p$. The Shakhov equilibrium distribution function f^S is given by the Maxwell distribution function f^M plus a heat flux correction term

$$\begin{aligned} f^S&=f^M\left[1+(1-\mathrm{Pr})\frac{\boldsymbol{c}\cdot\boldsymbol{q}}{5pRT}\left(\frac{c^2+\eta^2}{RT}-5\right)\right]=f^M+f_{\mathrm{Pr}},\\ f^M&=\frac{\rho}{(2\pi RT)^{3/2}}\exp\left(-\frac{c^2+\eta^2}{2RT}\right), \end{aligned} \tag{2}$$

where Pr is the Prandtl number and can be adjusted freely. For a monatomic gas considered in this work, Pr equals to 2/3. $\boldsymbol{c}=\boldsymbol{\xi}-\boldsymbol{U}$ is the peculiar velocity with $\boldsymbol{U}$ being the fluid velocity in two-dimensional space. R is the specific gas constant. The macroscopic state variables such as the density ρ, velocity $\boldsymbol{U}$, temperature T and heat flux $\boldsymbol{q}$ can be calculated by taking moments of the distribution function as,

$$\rho=\int f\mathrm{d}\boldsymbol{\xi}\mathrm{d}\eta,\quad \rho\boldsymbol{U}=\int\boldsymbol{\xi}f\mathrm{d}\boldsymbol{\xi}\mathrm{d}\eta,\quad \rho E=\tfrac{1}{2}\int(\xi^2+\eta^2)\mathrm{d}\boldsymbol{\xi}\mathrm{d}\eta,\quad \boldsymbol{q}=\tfrac{1}{2}\int\boldsymbol{c}(c^2+\eta^2)f\mathrm{d}\boldsymbol{\xi}\mathrm{d}\eta, \tag{3}$$

where $\rho E=(1/2)\rho U^2+C_vT$ is the total energy with C_v being the heat capacity [$(3/2)R$ for monatomic gasses]). The pressure is related to the density and temperature by $p=\rho RT$.

For two-dimensional problems considered in this work, the dependence of f on z-direction particle velocity η can be removed by introducing the following distribution functions,

$$\Phi=\begin{bmatrix} g\\ h\end{bmatrix}=\int_{-\infty}^{\infty}\begin{bmatrix}1\\ \eta^2\end{bmatrix}f(\boldsymbol{\xi},\eta,x,y,t)\mathrm{d}\eta. \tag{4}$$

Equation (1) can be therefore reduced by integrating it over the range of $[-\infty, \infty]$ with respect to η,

$$\frac{\partial \Phi}{\partial t} + \xi_x \frac{\partial \Phi}{\partial x} + \xi_y \frac{\partial \Phi}{\partial y} = -\frac{1}{\tau}\left[\Phi - \Phi^S\right], \tag{5}$$

where the reduced equilibrium distribution functions g^S and h^S in Φ^S are

$$\begin{aligned} g^S &= g^M \left[1 + (1 - \mathrm{Pr}) \frac{\boldsymbol{c} \cdot \boldsymbol{q}}{5pRT} \left(\frac{c^2}{RT} - 4\right)\right], \\ h^S &= g^M \left[1 + (1 - \mathrm{Pr}) \frac{\boldsymbol{c} \cdot \boldsymbol{q}}{5pRT} \left(\frac{c^2}{RT} - 2\right)\right] RT, \\ g^M &= \frac{\rho}{2\pi RT} \exp\left[-\frac{c^2}{2RT}\right]. \end{aligned} \tag{6}$$

The conservative macroscopic variables can be computed from these reduced distribution functions as

$$\rho = \int g \mathrm{d}\boldsymbol{\xi}, \quad \rho \boldsymbol{U} = \int \boldsymbol{\xi} g \mathrm{d}\boldsymbol{\xi}, \quad \rho E = \frac{1}{2}\int (\xi^2 g + h) \mathrm{d}\boldsymbol{\xi}, \tag{7}$$

and the heat flux can be computed as

$$\boldsymbol{q} = \frac{1}{2}\int \boldsymbol{c}(c^2 g + h) \mathrm{d}\boldsymbol{\xi}. \tag{8}$$

We make a comment here that even though the Shakhov model is used here for approximating the collision term, but other models have also been proposed such as the ellipsoidal statistical Bhatnagar-Gross-Krook (ES–BGK) [34] and the unified model of both Shakhov model and ES–BGK model [35]. More importantly, for thermally induced flow simulations, the ES-BGK model is reported to perform better than the Shakhov model in terms of the agreement of the temperature field to the full Boltzmann equation solution [36, 35], which is different from the cases of strong non-equilibrium high-speed flows, for which the Shakhov model is more accurate [37, 17]. Nevertheless, the numerical results for thermally induced problems in this study show that the agreements to the DSMC solution are still quite well using the Shakhov model.

2.2. Discrete unified gas kinetic scheme

The discrete unified gas kinetic scheme (DUGKS) is a finite-volume scheme for the discrete-velocity Boltzmann model equations. The governing equation Eq. (5) is firstly discretized in the velocity space with a set of chosen discrete velocity points $\{\boldsymbol{\xi}_\alpha, \alpha = 1, 2, ..., M\}$,

$$\frac{\partial \Phi_\alpha}{\partial t} + \boldsymbol{\xi}_\alpha \cdot \boldsymbol{\nabla} \Phi_\alpha = -\frac{1}{\tau}[\Phi_\alpha - \Phi_\alpha^S] \equiv \Omega_\alpha, \tag{9}$$

where Φ_α and Φ_α^S are the distribution function and equilibrium distribution function with discrete velocity $\boldsymbol{\xi}_\alpha$. Equation (9) is then discretized in the spatial space with the following cell-centered finite-volume scheme [28],

$$\Phi_{\alpha,k}^{n+1} - \Phi_{\alpha,k}^n + \frac{\Delta t}{|V_k|}\mathcal{F}_{\alpha,k}^{n+1/2} = \frac{\Delta t}{2}[\Omega_{\alpha,k}^{n+1} + \Omega_{\alpha,k}^n], \quad k = 1, 2, \ldots, N, \tag{10}$$

where $\Phi^n_{\alpha,k}$ is the cell averaged value of Φ_α in cell k at time level t^n, $|V_k|$ is the volume of the cell k, N is total number of cells and $\Delta t = t^{n+1} - t^n$ is the time step.

The flux $\mathcal{F}^{n+1/2}_{\alpha,k}$ is evaluated at middle time step at the cell face center by [28],

$$\mathcal{F}^{n+1/2}_{\alpha,k} = \sum_l \boldsymbol{\xi}_\alpha \cdot \boldsymbol{S}_{k,l} \Phi^{n+1/2}_{\alpha,k,l}, \tag{11}$$

where $\boldsymbol{S}_{k,l}$ is the surface vector of face l belonging to cell k, and $\Phi^{n+1/2}_{\alpha,k,l}$ is the distribution function at the center of face l at the middle time step. The distribution functions at cell faces are constructed by integrating the governing equation locally along the characteristic line that ends at the cell face center $\boldsymbol{x}_f$ from t^n to $t^{n+1/2}$,

$$\Phi^{n+1/2}_\alpha(\boldsymbol{x}_f) - \Phi^n_\alpha(\boldsymbol{x}_f - \boldsymbol{\xi}_\alpha s) = s/2 \left[\Omega^{n+1/2}_\alpha(\boldsymbol{x}_f) + \Omega^n_\alpha(\boldsymbol{x}_f - \boldsymbol{\xi}_\alpha s) \right], \tag{12}$$

where $s = t^{n+1/2} - t^n$ is the half time step. Equation (12) can be rewritten in an explicit form by introducing $\bar{\Phi} = \Phi - s/2\Omega$ and $\bar{\Phi}^+ = \Phi + s/2\Omega$,

$$\bar{\Phi}^{n+1/2}_\alpha(\boldsymbol{x}_f) = \bar{\Phi}^{+,n}_\alpha(\boldsymbol{x}_f - \boldsymbol{\xi}_\alpha \Delta t/2), \tag{13}$$

where $\bar{\Phi}^{+,n}_\alpha(\boldsymbol{x}_f - \boldsymbol{\xi}_\alpha \Delta t/2)$ is interpolated using first order Taylor expansion from the upstream cell center [28, 29]. After getting $\bar{\Phi}^{n+1/2}_\alpha(\boldsymbol{x}_f)$, the macro variables at the cell face $W^{n+1/2}(\boldsymbol{x}_f)$ can be obtained by taking moments of $\bar{\Phi}^{n+1/2}_\alpha(\boldsymbol{x}_f)$ due to the compatibility condition [28]. Then the original distribution function $\Phi^{n+1/2}_\alpha(\boldsymbol{x}_f)$ can be recovered from the relation of $\bar{\Phi}$ and Φ as [28]

$$\Phi^{n+1/2}_\alpha(\boldsymbol{x}_f) = \frac{2\tau}{2\tau + s} \bar{\Phi}^{n+1/2}_\alpha(\boldsymbol{x}_f) + \frac{s}{2\tau + s} \Phi^{S,n+1/2}_\alpha(\boldsymbol{x}_f). \tag{14}$$

Equation (10) can be rewritten in the following explicit form by introducing another two transformed distribution functions, $\tilde{\Phi} = \Phi - \Delta t/2\Omega$ and $\tilde{\Phi}^+ = \Phi + \Delta t/2\Omega$,

$$\tilde{\Phi}^{n+1}_{\alpha,k} = \tilde{\Phi}^{+,n}_{\alpha,k} - \frac{\Delta t}{|V_k|} \mathcal{F}^{n+1/2}_{\alpha,k}. \tag{15}$$

In the actual implementation, $\tilde{\Phi}$ is tracked instead of Φ. $\tilde{\Phi}^+$ and $\bar{\Phi}^+$ are calculated from $\tilde{\Phi}$ by [28]

$$\bar{\Phi}^+ = \frac{2\tau - s}{2\tau + \Delta t} \tilde{\Phi} + \frac{3s}{2\tau + \Delta t} \Phi^S, \quad \tilde{\Phi}^+ = \frac{2\tau - \Delta t}{2\tau + \Delta t} \tilde{\Phi} + \frac{2\Delta t}{2\tau + \Delta t} \Phi^S. \tag{16}$$

The detailed algorithm of the DUGKS can be find in Ref. [28].

The time step in the DUGKS is determined by the Courant-Friedrichs-Lewy (CFL) condition,

$$\Delta t = \alpha \left(\frac{\Delta x}{|\boldsymbol{U}| + |\boldsymbol{\xi}|} \right)_{\min}, \tag{17}$$

where $0 < \alpha < 1$ is the CFL number and Δx is the distance between the centers of two adjacent cells that share an interface. Appropriate velocity grid that can fully resolve the distribution function

is chosen according to a prior estimation of the deviation of the distribution function from the local equilibrium distribution function. The moments are approximated from the discrete distribution function using a certain numerical quadrature. For low Kn (Kn ≤ 0.1) cases, the distribution function is near the Maxwell distribution and smooth in the velocity space, thus we choose the half-range Gauss-Hermit quadrature which can well capture the distribution function. On the other hand, for higher Kn (Kn > 0.1) cases, the distribution function may be irregular and even discontinuous, and we choose the Newton-Cotes quadrature with uniform discrete velocity grid such that we can refine the velocity mesh more easily than using the Gauss quadrature. Specifically, the bound of the Newton-Cotes type of velocity grid is chosen to be $[-4\sqrt{2RT_{\rm ref}}, 4\sqrt{2RT_{\rm ref}}]$. The velocity grid has to be fine enough to resolve the non-smooth distribution function near the origin of the velocity space which is a typical phenomenon in thermally induced rarefied flows [38]. Thus the total number of discrete velocities can be very large due to the using of a uniform grid. Using a non-uniform grid with most quadrature points locates near the origin (see e.g., in Ref. [38]) or an optimized discrete velocity set [8, 39] can mitigate this problem. Another way to reduce the number of discrete velocities is to apply the conservative integration or correction for the moments (see e.g., in Ref. [40, 41]).

As the DUGKS is an explicit scheme, for steady problems, the flow field will be assumed to be steady only if the average relative change of the macro fields in two-successive steps are less than a given tolerance ϵ (10^{-8} in this study),

$$\varepsilon^n = \frac{\sum_k |\mathcal{W}_k^{n+1} - \mathcal{W}_k^n|}{\sum_k \mathcal{W}_k^n} < \epsilon, \quad \text{for} \quad \mathcal{W} \in \{\rho, \boldsymbol{U}, T\}, \tag{18}$$

where the summations are taken over all cells.

2.3. Analysis of the numerical flux in the DUGKS

The distinct feature of the DUGKS is that the flux of distribution function is obtained from the local characteristic solution of the governing equation itself, instead of directly interpolated from the distribution function at nearby cell centers as usually done in classical DOM schemes.

The exact solution of governing equation at cell face center is

$$\Phi_\alpha^{n+1/2}(\boldsymbol{x}_f) = \Phi_\alpha^n(\boldsymbol{x}_f - s\boldsymbol{\xi}_\alpha) + \int_0^s \Omega_\alpha(\boldsymbol{x}_f - s\boldsymbol{\xi}_\alpha + t'\boldsymbol{\xi}_\alpha, t^n + t')dt'. \tag{19}$$

The first and second term on the right-hand side represents the free streaming and collision effect along the characteristic line, respectively. In the DUGKS, the integration of the collision term in Eq. (19) is approximated using the trapezoidal rule, so the error introduced is $O(\Delta t^3)$. The first term on the right-hand side can be viewed as obtained by second-order interpolation. Thus the error is $O(\Delta x^2)$. The overall error in the evaluation of the distribution function at middle time step is

therefore $O(\Delta x^2) + O(\Delta t^3)$, and the error in the approximation of distribution function flux

$$F = \frac{1}{\Delta t}\int_0^{\Delta t} \Phi_\alpha(\boldsymbol{x}_b, t^n + t')dt' \tag{20}$$

will be the order of $O(\Delta x^2) + O(\Delta t^2)$ as the middle point rule is employed. Note that the integration of the collision term, i.e., the second term of the right-hand side of Eq. (19) is of order $O(\Delta t)$ and it contributes to the physical flux [42]. If we totally ignore this term, however, like classic explicit schemes where certain interpolation scheme or total variation diminishing (TVD) schemes are used, the time-step related error in the numerical flux will be the order of $O(\Delta t)$. The direct consequence is that the time step Δt should be set to a much smaller value than the mean collision time τ to suppress the numerical error which appears as numerical dissipation [43, 44]. For rarefied flows, this is not a problem since τ is relatively large and the CFL condition limited Δt is usually much smaller than τ. But for near continuum flows, where τ is very small, this requirement of $\Delta t \ll \tau$ make the computation intractable. By computing the cell face distribution from the governing equation, both the free transport and collision effect are considered naturally in the evaluation of distribution function flux in the DUGKS, which insures the DUGKS can capture the both the free-molecular limit and the continuum limit of the kinetic equation. In the free-molecular limit, $\Delta t/\tau \to 0$, from Eq. (12), we can get the middle time distribution function at cell face as

$$\Phi_\alpha^{n+1/2}(\boldsymbol{x}_f) = \Phi_\alpha^n(\boldsymbol{x}_f - \boldsymbol{\xi}_\alpha s), \tag{21}$$

which is the exactly the solution the free-molecular Boltzmann equation. While in the continuum limit where $\Delta t \gg \tau$, the solution is (refer to the details in Appendix B of Ref. [27]),

$$\Phi_\alpha^{n+1/2}(\boldsymbol{x}_f) = \Phi_\alpha^{n,S}(\boldsymbol{x}_f) - \tau(\partial t + \boldsymbol{\xi}_\alpha \cdot \boldsymbol{\nabla})\Phi_\alpha^{n,S}(\boldsymbol{x}_f) + s\partial_t \Phi_\alpha^{n,S}(\boldsymbol{x}_f), \tag{22}$$

which is the just Chapman-Enskog approximation of the Navier-Stokes equation. It means the DUGKS can reduce to a scheme for the Navier-Stokes equation in the continuum limit. Here we also note some unified schemes have also been proposed using other approaches. For example, the gas-kinetic unified algorithm (GKUA) employs a Strang-splitting treatment of the collision/convection terms together with a high-order time-integration scheme of the kinetic equation and is demonstrated to be able to simulate near continuum flow effectively [45, 17].

3. Numerical test cases

In this section, we apply the DUGKS to the simulation of several kinds of TINE flows. In all of the cases, the gas medium is modeled as a argon gas with its molecular mass $m = 6.63 \times 10^{-26}$kg, hard-sphere diameter $d = 4.17 \times 10^{-10}$m and temperature dependent viscosity as $\mu = \mu_{\text{ref}}(T/T_{\text{ref}})^\omega$,

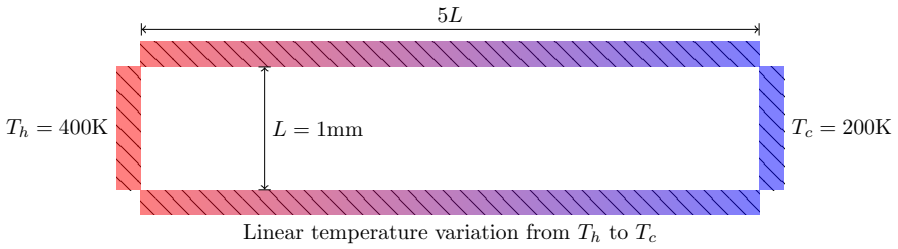

Figure 1: Thermal creep flow in a closed channel.

where $\omega = 0.81$ corresponding to the variable hard-sphere (VHS) collision model of the argon gas. The reference viscosity μ_{ref} is calculated also through the VHS model [46]

$$\mu_{\text{ref}} = \frac{15\rho_{\text{ref}} R T_{\text{ref}} \lambda_{\text{ref}}}{(5-2\omega)(7-2\omega)} \sqrt{\frac{\pi}{2RT_{\text{ref}}}}, \tag{23}$$

where ρ_{ref}, λ_{ref} and T_{ref} are the reference density, mean free path and temperature respectively. The mean free path is related to the gas density by $\lambda_{\text{ref}} = m/(\sqrt{2}\pi d^2 \rho_{\text{ref}})$ [46]. The DUGKS results are calculated using the recently developed dugksFoam solver [47]. The DSMC results used for comparison are obtained with the well-validated open source solver dsmcFoam [48] unless otherwise stated. The VHS model is used in the dsmcFoam for the inter-molecular collision. An average of 50 simulated particles in each cell are used for all of the cases, which is larger than common practices [46] to account for the extremely low signal-to-noise ratio of the thermally induced flows.

3.1. Thermal creep flow in a closed channel

At rarefied condition, gas near a wall with tangential surface temperature gradient start to creep in the direction from cold towards hot. This phenomenon is referred as thermal creep flow or thermal transpiration [49]. In this study, we consider a flow configuration as illustrated in Fig. 1. The flow geometry is a two-dimensional straight channel with closed ends and a length-to-width ratio of 5. The width of the channel is $L = 1\,\text{mm}$. The left and right ends are kept at a lower and higher temperatures of $T_c = 200K$ and $T_h = 400\,\text{K}$, respectively, while the lateral sides are imposed a linear temperature distribution that varies from T_c at the left to T_h at the right. T_h is used as the reference temperature, i.e., $T_{\text{ref}} = T_h$. All of the channel walls are assumed to be diffusive boundaries. The gas in the channel is initialized with a uniform density and a linearly varied temperature as same as the lateral walls. The Knudsen number is defined based on the initial uniform density field and the channel width. We note that the same problem has been simulated before by various kinds of methods, such as the fast spectral method (FSM) [38], the unified gas kinetic scheme (UGKS) [50] and information-preservation DSMC (IP–DSMC) [20].

Four cases corresponding to $\text{Kn} = 0.01$, 0.1, 1 and 10 are simulated by both the DUGKS and DSMC methods. For both the DUGKS and DSMC simulations, we use a uniform structured mesh with 50 by

250 square cells. The velocity space in the DUGKS is discretized using 16×16 and 28×28 half-range Gauss-Hermit quadrature points for the cases of Kn = 0.01 and 0.1, respectively, while 161×161 and 201×201 uniformly distributed Newton-Cotes quadrature points for the cases of Kn = 1 and 10, respectively. For the case of Kn = 10, the non-equilibrium effect is quite strong and it is further enhanced by the large temperature difference between the channel ends. It is desirable to use such a fine discrete velocity grid (201×201) to adequately resolve the irregular distribution function near the origin of the velocity space since we are using the uniformly spaced discrete velocity points. Using a non-uniform discrete velocity grid [38, 51] should reduce the total number of discrete velocities and therefore the computational cost.

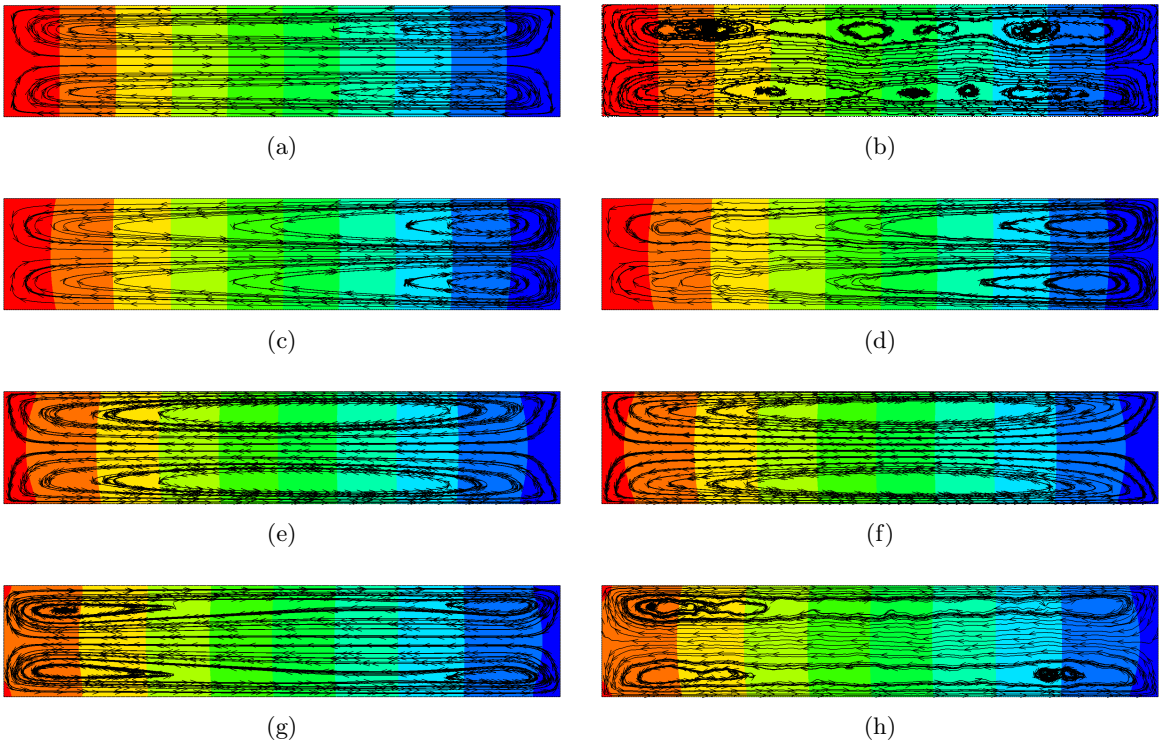

Figure 2: Temperature contours and streamlines for the thermal creep flow case. Left panel: DUGKS results. Right panel: DSMC results. Knudsen numbers in each panel from top to bottom are Kn = 0.01, 0.1, 1 and 10. The non-dimensional contour levels in each contour plot are from 0.65 to 0.95 with a uniform step of 0.05.

The temperature fields and streamlines at various Knudsen numbers predicted by the DUGKS and DSMC simulations are presented in Fig. 2 side-by-sides. We can see from Fig. 2 the good agreements between the DUGKS and DSMC results, especially in terms of the temperature fields. For the case of Kn=0.01, the statistic noise of the velocity field predicted by DSMC method is still significant, despite a very long time averaging has been conducted. Nevertheless, the overall flow patterns predicted by the two methods are still very similar to each other at this low Knudsen number. For the case of Kn = 1, the vortex center position predicted by the DUGKS is obviously more close to the horizontal centers

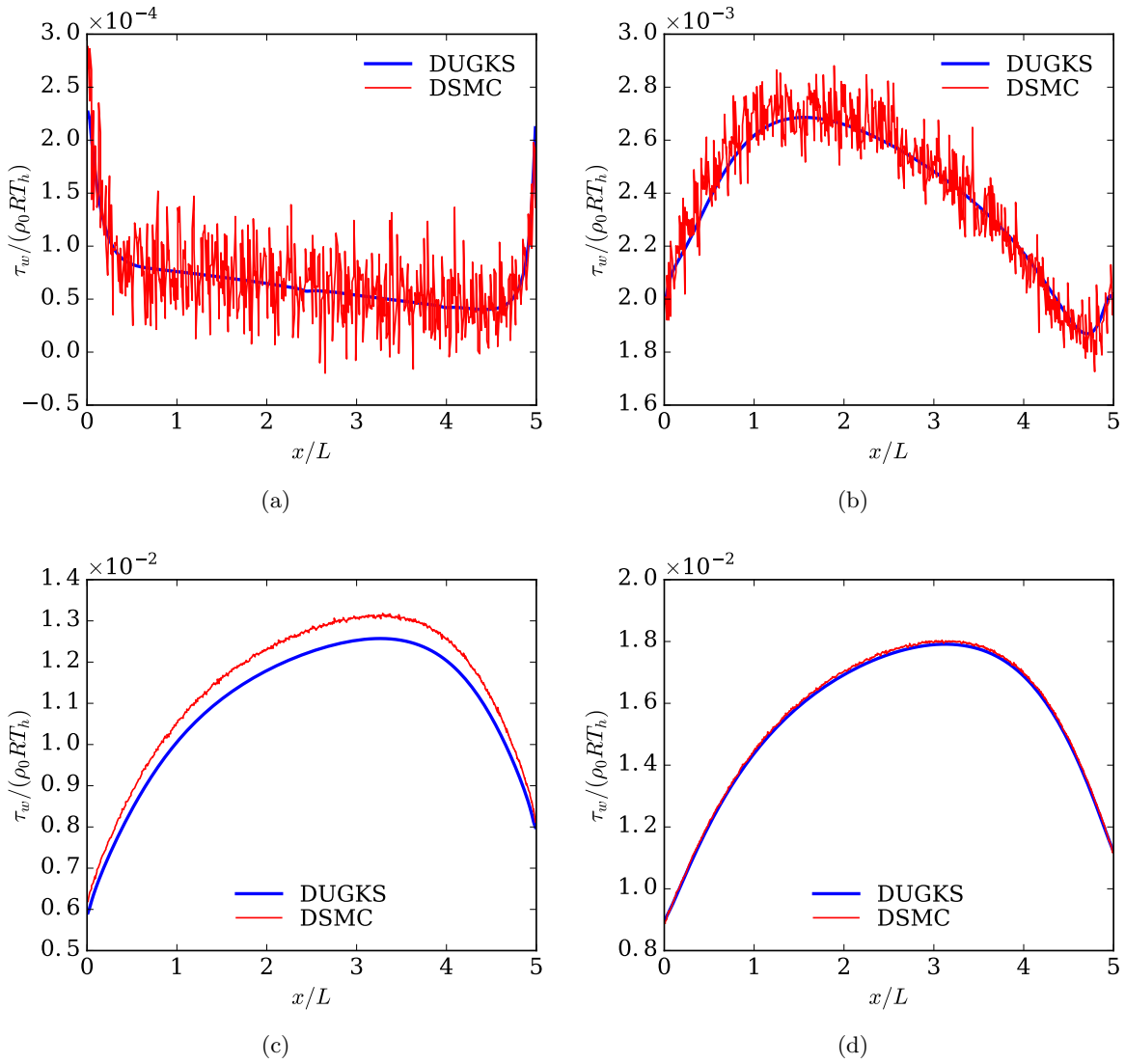

Figure 3: Non-dimensional shear stress along the later side of the channel for the thermal creep flow case. (a) Kn = 0.01, (b) Kn = 0.1, (c) Kn = 1, (d) Kn = 10.

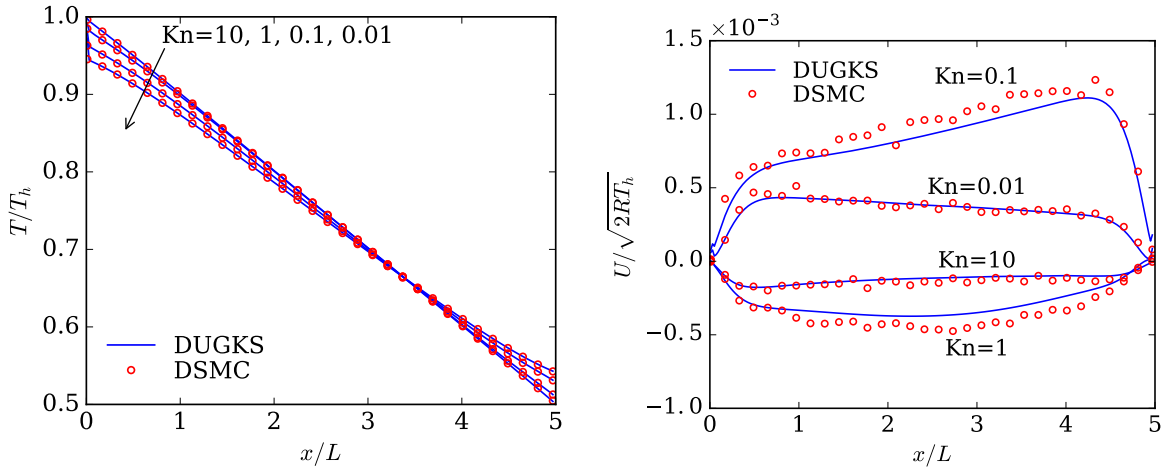

Figure 4: Non-dimensional temperature (a) and U-velocity (b) profiles along the horizontal center line of the therm creep flow case.

of the channel than the DSMC result, whereas, at lower or higher Knudsen numbers, such difference cannot be observed. The difference at this Knudsen number can be attributed to the difference between the Shakhov model equation used by the DUGKS and the full Boltzmann equation (VHS model in this study) in DSMC method. In the transition regime, the effect of different treatments on the collision term of the Boltzmann equation is more significant than in the other flow regimes. In the slip regime, the kinetic nature of the flow vanishes, while in the free molecular flow regime, the contribution of the collision term is negligible. Thus in both regimes, the flow field is insensitive to the choice of model for the collision term. A recent study [38] has shown that for thermally driven flows, even solved using the full Boltzmann equation, the velocity field is still affected by the specific collision model significantly. To compare the results further, we plot the shear stress along the lateral side of the channel in Fig. 3 and the temperature as well as the horizontal velocity profiles along the horizontal central line in Fig. 4. From Fig. 3 and Fig. 4(b), we can observe that it is again in the case of Kn = 1 that the difference between the DUGKS and DSMC results is more profound. While in all of the cases, the temperature profiles agree quite well as indicated in Fig. 4(a).

3.2. Flow induced by a hot microbeam immersed near a cold substrate

In this case, we consider a flow induced by the configuration as illustrated by Fig. 5. This configuration is a two-dimensional abstraction (or cross section) of a long heated microbeam immersed in a pipe with rectangular cross section and a colder surface temperature. At rarefied condition, when the separation between a heated object and a nearby substrate is comparable to the mean free path, a low-speed flow will develop around the heated object and hence a net force will be exerted on the object. This kind of force is called Knudsen force and has been recently studied by many experiments

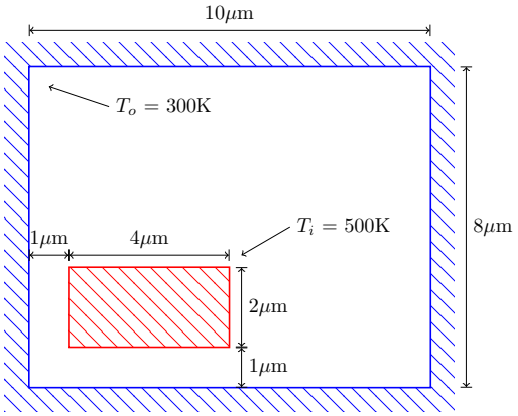

Figure 5: Heated microbeam (cross section) in a cavity.

and numerical analyses [52–54, 13, 3, 22], possibly due to its important applications in Microelectromechanical Systems (MEMS). In this study, the microbeam and the outer pipe wall serve as the heated object and the cold substrate, respectively. As the surfaces of the microbeam and the substrate are maintained at *uniform* temperatures, the flow is fundamentally different from the thermal creep flow described in the above subsection. It can be classified as combined effect of thermal stress flow and thermal edge flow [49] due to the inhomogeneity of the temperature gradient and the sharp corners of the microbeam.

The temperature of the microbeam surface is kept at $T_i = 300\,\mathrm{K}$ and the substrate at $T_o = 500\,\mathrm{K}$. The sizes and the arrangements of the microbeam and substrate are obvious from the figure. All of the solid walls are assumed to be diffusive boundaries. The reference temperature is $T_{\mathrm{ref}} = 400\,\mathrm{K}$. The overall Knudsen number is defined using the narrowest separation between the microbeam and the substrate which is 1 µm, and the mean free path which is defined using the initial uniform gas density. We consider three Knudsen numbers in this case, i.e., Kn $= 0.1,\ 1$ and 10. For all of the cases, the discrete velocity space is discretized in the range of $[-4\sqrt{2RT_{\mathrm{ref}}}, 4\sqrt{2RT_{\mathrm{ref}}}]^2$ with uniform points. For the cases of Kn $= 0.1$ and 1, 101×101 points are used, while for the case of Kn $= 10$, a finer grid with 201×201 points are used due to the more pronounced non-equilibrium effect at this high Knudsen number case. Three physical meshes with different resolutions are used for the three cases. A total of 85600, 25300 and 2960 rectangular cells are used in the meshes for the cases of Kn $= 0.1,\ 1$ and 10, respectively, with the smallest cells padding around the microbeam wall and the outer cavity wall.

The velocity magnitude fields and the streamlines for each of the cases are presented in Fig. 6, together with the DSMC results simulated using an in-house code (see in Acknowledgments). From the figures, we can see the quite well agreements between the DUGKS and DSMC results, and the rich vortexes developed at the corners of the microbeam. The maximum velocity magnitude is about 2.2m/s and appears at the upper right corner of the microbeam in the case of Kn $= 1$. The tiny vortexes

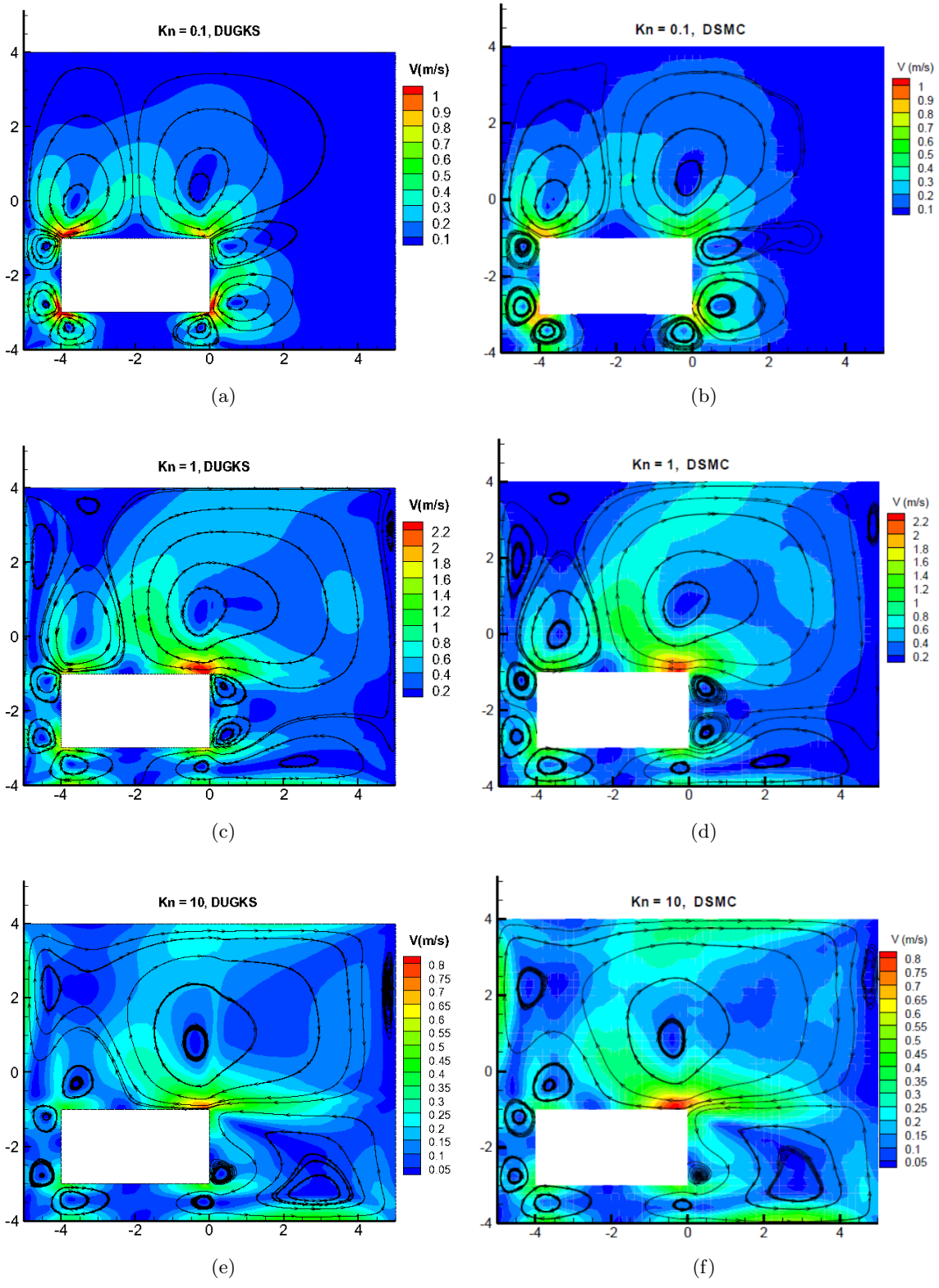

Figure 6: Temperature contours and streamlines for the microbeam flow case. Left panel: DUGKS results. Right panel: DSMC results. Knudsen numbers in each panel from top to bottom are Kn = 0.1, 1 and 10.

near the outer wall in the case of Kn = 1 have been captured by both methods. Figure 7 shows the non-dimensional shear stress and normal stress distribution along the surface of the microbeam. Good agreements can be observed from the figures. It also reveals that as the Knudsen number decreases, the non-uniformities of both the normal stress and the shear stress along the microbeam surface tend to more obvious, and the stresses are accumulated near at the corner of the microbeam.

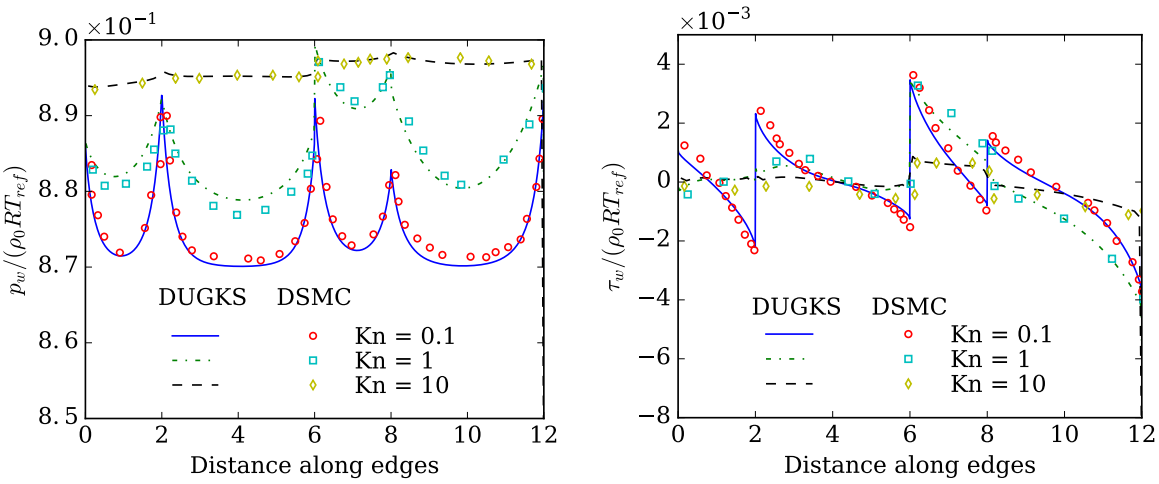

Figure 7: Non-dimensional normal stress (a) and shear stress (b) along the surface of the microbeam. The x-axis represents the path length along the microbeam surface starting from the left-upper corner with a counter-clock direction.

3.3. Radiometric flow

In this case, we consider another thermally induced flow generated by a small plate with differentially heated sides placed in a chamber. Such flow is called radiometric flow and the force acting on the small plate is called radiometric force [2]. This kind of force is known to be the driven mechanism of the radiometer invented by William Crookes in the 19th century. The origin of the radiometric force has long been a debate ever since the late 1900s and has attracted the interest of many prominent scientists [2]. Not until recently, direct computations based upon Boltzmann model equations have made it possible to study such flow phenomenon in detail [13, 55]. In this testing case, the flow configuration is stretched in Fig. 8. The outer chamber size is 45 cm × 45 cm and the small plate enclosed has a size of 0.95 cm × 3.81 cm and is placed at the geometric center of the chamber which is the origin of the coordinate system. The temperatures of plate's left and right surface are kept at $T_l = 419\,\mathrm{K}$ and $T_r = 394\,\mathrm{K}$, respectively. Both the upper and lower side of the plate is maintained at 400 K. The chamber surface is kept at $T_c = 300\,\mathrm{K}$. All of the boundaries are treated as diffusive walls. The Knudsen number of the system is defined using the ratio of the reference mean free path λ_{ref} to the plate height $L = 3.81\,\mathrm{cm}$, where λ_{ref} is defined using the initial uniform gas density. Due to the

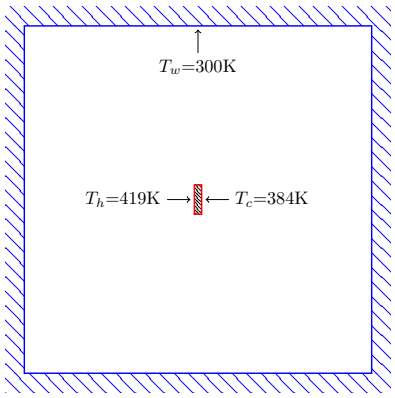

Figure 8: Geometry configuration of the radiometric flow in a closed chamber.

symmetry of the flow domain in the vertical direction, only the upper half-domain is computed. Two Knudsen numbers, i.e. Kn = 0.1 and 1 are considered. An unstructured mesh with 22790 quadrangle elements is used and it is refined near the surface of the plate. To be more specific, a total number of 50 cell faces are uniformly padded along the surface of the half plate in the computational domain. For the case of Kn = 0.1, at set of 28×28 half-range Gauss–Hermit quadrature points is used in the discretization of the velocity space, while for the case of Kn = 1, 81×81 uniform points in the range of $[-4\sqrt{2RT_{\text{ref}}}, 4\sqrt{2RT_{\text{ref}}}]^2$ and Newton–Cotes quadrature are employed.

The temperature fields and streamlines predicted by both the DUGKS and DSMC methods are presented in Fig. 9. We can see for the case of Kn = 1, the overall agreements between the DUGKS and DSMC result are quite well in terms of both the temperature and the velocity fields. While in the case of Kn = 0.1, the agreements are less satisfactory. At this lower Knudsen number, the vortex shapes predicted by the two methods at the right side of the plate exhibit small difference. The temperature field predicted by the DUGKS near the vicinity of the plate is slightly higher than that in the DSMC result. The differences here can be explained by the fact that the Shakhov model used in the DUGKS is different from the full Boltzmann collision term used in the DSMC method, and such difference is more pronounced in the transition regime. Another reason is that the statistic noise in the DSMC results is still quite large as the temperature difference across the plate is very small, even though a long time averaging has been conducted in the DSMC simulation. Figure 10 presents the pressure (normal stress) difference between the left and right side of the plate along the vertical direction, which is the main contribution to the radiometric force as having been analyzed [13, 55]. We can see the at the higher Knudsen number (Kn = 1), the left/right pressure difference is nearly uniform along the plate surface in the vertical direction, and the DUGKS and DSMC results agree well. At the lower Knudsen number (Kn = 0.1), the left/right pressure difference is non-uniform along the plate edge and takes larger value near the ends (top and bottom) of the plate. But the smallest

pressure difference (at the center of the plate) is still larger than that in the case of Kn = 1. The DSMC results at Kn = 0.1 are systematically higher than that of the DUGKS results and exhibit quite a large statistic noise.

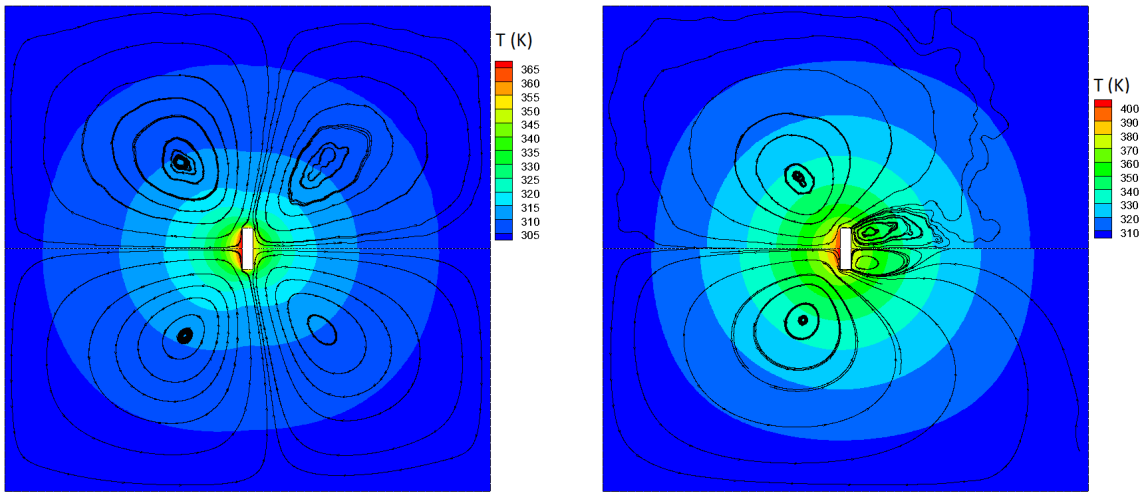

(a) (b)

Figure 9: Temperature field and streamlines of the radiometric flow case. Left: Kn = 1. Right: Kn = 0.1.

3.4. Flows induced by temperature discontinuity

The last case is the flow in a square cavity induced by temperature discontinuities at the cavity boundaries. The geometric configuration and boundary conditions are sketched in Fig. 11. The side length of the square cavity is L. The temperature on the top wall is maintained at T_h, while on other walls it is maintained at a lower temperature T_c. Thus the wall temperature is discontinued at the upper corners of the cavity. Such temperature discontinues will induce gas circulations in the cavity as having been investigated in Refs. [56, 20, 50]. All of the walls are treated as diffusive boundaries. The reference mean free path λ_{ref} is calculated from the initial uniform density, and the reference temperature is set to be $T_{\text{ref}} = 300\,\text{K}$. The Knudsen number is defined as the ratio of λ_{ref} to L. Four cases corresponding to Kn = 0.001, 0.1, 1 and 10 are computed. For all of the cases, we use a mesh with 60×60 uniform cells in the physical space. The velocity grids for the cases of Kn = 0.001 and Kn = 0.1 are of half-range Gauss-Hermit type with 12×12 and 28×28 points, respectively. While for the case of Kn = 1 and 10, we use 161^2 and 201^2 uniform points respectively with Newton–Cotes quadrature.

For the case of Kn = 0.1, 1 and 10, we compare our results with DSMC solutions. A relatively higher temperature difference between the top wall and other walls, i.e., $T_c = 200\,\text{K}$ and $T_h = 400\,\text{K}$ is used so we can obtain the DSMC solution with minimal effort. The temperature and velocity fields

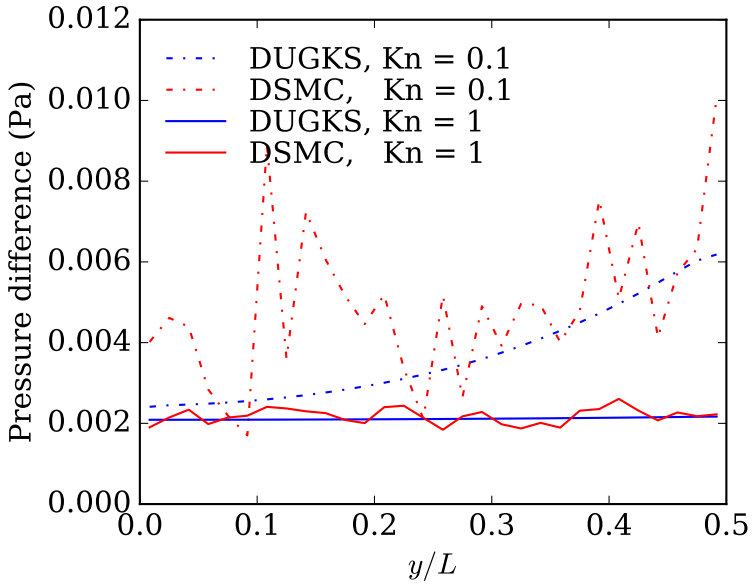

Figure 10: Distribution of normal pressure (stress) difference between the hot and cold sides of the plate (Pa) along the vertical direction. Only a half region is shown due to the symmetrical configuration.

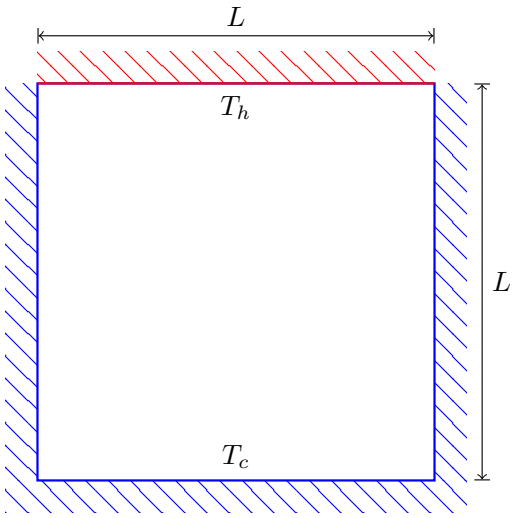

Figure 11: Geometry configuration of the flow induced by temperature discontinuities.

predicted by both the DUGKS and DSMC methods are shown in Fig. 12(b)-(d). The temperature and velocity profiles along the center lines of the cavity are present in Fig. 13.

We can see like other cases in this study, the overall agreement between the two results, especially in terms of the temperature field, is quite well. The detailed vortex shape and vortex center locations exhibit obvious differences among the two results, particularly in the case of Kn = 0.1 and 1. The velocity profiles in Fig. 13(c)-(d) present the differences of the velocity field between the DUGKS and DSMC results more clearly. As have been explained in Sec. 3.1, such discrepancies can be explained by the difference collision models used in the DUGKS and DSMC methods.

In the case of Kn = 10, the velocity field predicted by the DUGKS method is unsmooth and unphysical vortexes appear in various locations. These numerical errors can be attributed to the sharp discontinuity of the distribution function due to the large temperature discontinuity at the upper corners at the highly rarefied condition and the limited resolution of the discrete velocity grid.

For the case of Kn = 0.001, we compare our results with the analytical solution based on the heat equation. In such low Knudsen number condition, the flow approaches its continuum limit described by the Navier-Stokes-Fourier equation. Provided the temperature difference at the corner is small, the vanishing but still nonzero [56] thermally induced velocity field has a negligible effect on the temperature field, thus the temperature field is essentially governed by the heat equation. A recent study based on the ES–BGK model equation has also confirmed the validity of using the heat equation to predict the temperature field [57]. In our simulation for the case of Kn = 0.001, the temperature difference is 1 K, and we set $T_h = 301\,\mathrm{K}$, $T_c = 300\,\mathrm{K}$ and $T_{\mathrm{ref}} = 300\,\mathrm{K}$. The analytical solution based on heat equation is given by [58],

$$\theta(x,y) = \frac{2}{\pi}\sum_{n=1}^{\infty}\frac{(-1)^{n+1}+1}{n}\sin(n\pi x/L)\frac{\sinh(n\pi y/L)}{\sinh(n\pi)}, \tag{24}$$

where θ is the normalized temperature defined as $\theta = (T-T_c)/(T_h-T_c)$ and the origin of the coordinate system is taken as the lower left corner of the cavity. The DUGKS solution together with the solution obtained from Eq. (24) is presented in Fig. 12(b), from which we can see quite well agreement has been achieved.

4. Summary

In this paper, the application of the discrete unified gas kinetic scheme for simulating thermal induced non-equilibrium flows has been explored. Fours types of thermally induced flows have been simulated in a wide range of Knudsen numbers and the results have been validated using DSMC results. The results show that DUGKS can be faithfully used for thermally induced low-speed flows.

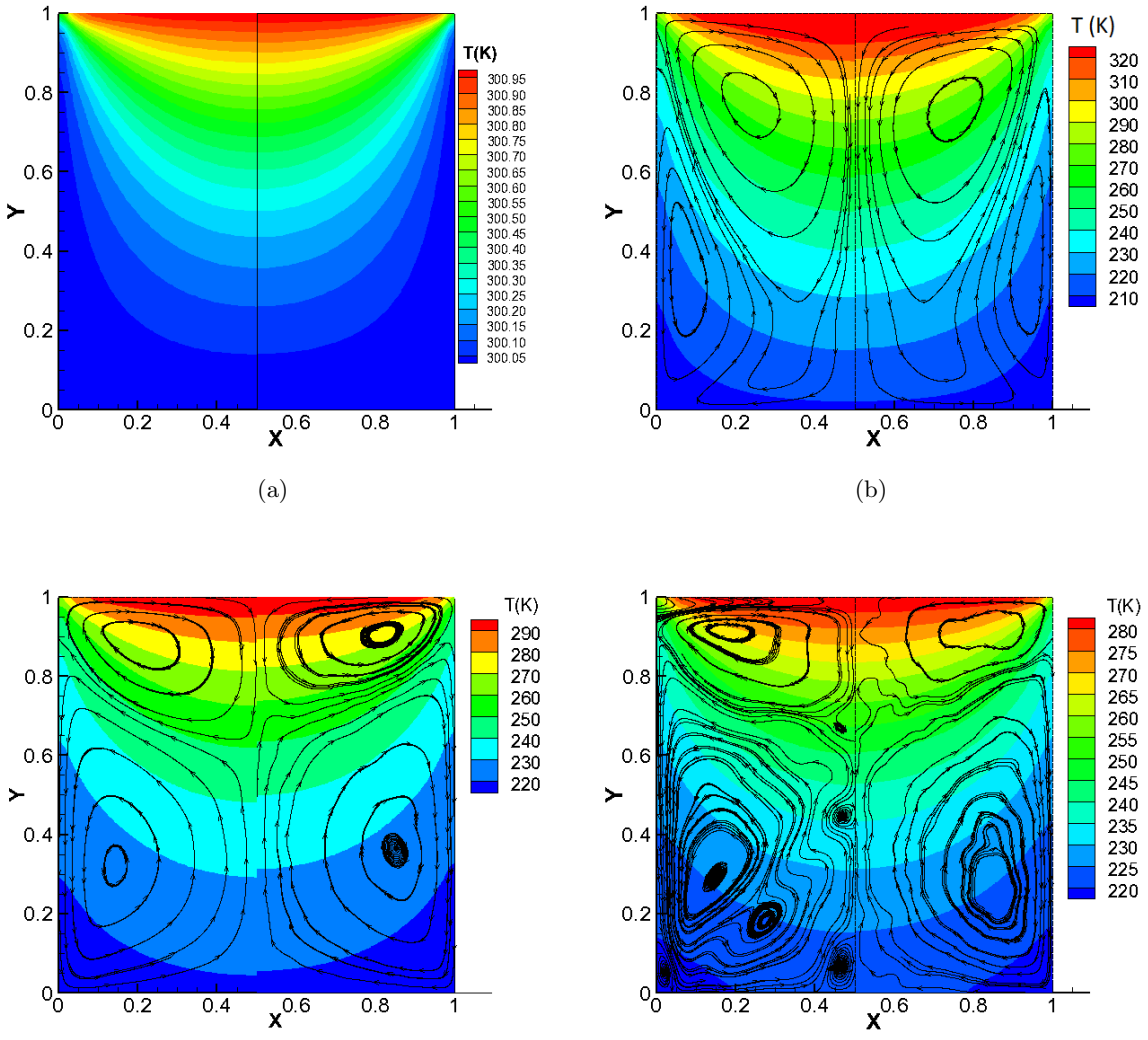

(a) (b)

(c) (d)

Figure 12: Temperature field and streamlines [only in (b), (c), (d)] of the temperature discontinuity induced flow case. Sub-figure (a) is for the case of Kn = 0.001, left and right half are the DUGKS solution and the analytical solution based on heat equation [(24)]. Sub-figures (b), (c) and (d) correspond to the cases of Kn = 0.1, 1 and 10, respectively. In each sub-figure, left and right half are results using the DUGKS and DSMC method, respectively.

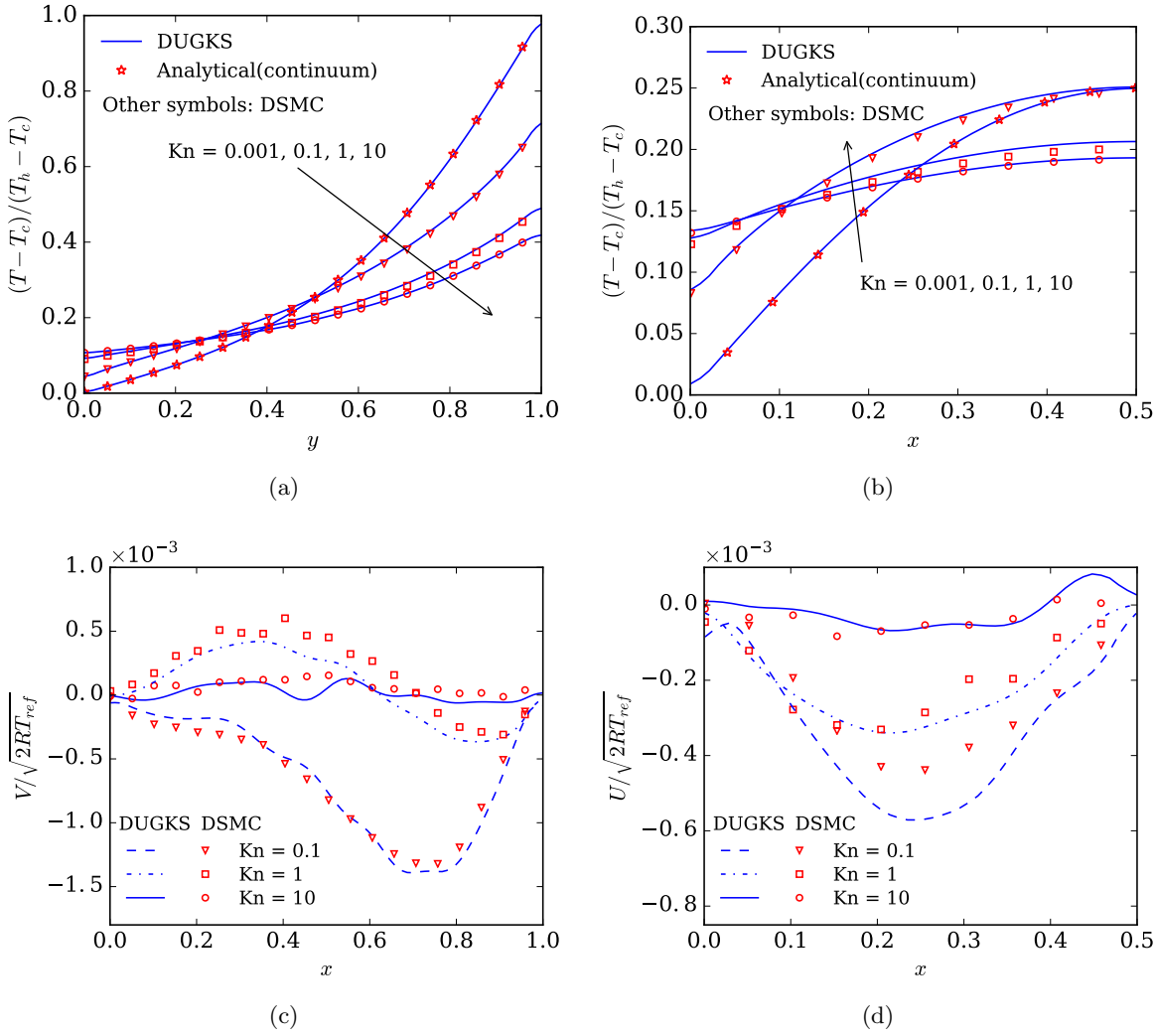

Figure 13: Temperature field and velocity profiles of the temperature discontinuity induced flow case. (a) Temperature profiles along the vertical center line. (b) Temperature profiles along the horizontal center line. (c) V-velocity profiles along the vertical center line. (d) U-velocity profiles along the horizontal center line.

Due to the coupled treatment of the collision and free-transport effects in the evaluation of distribution function flux, the scheme can handle both the rarefied flows and near continuum flows or continuum flows in a unified manner without changing the physical mesh resolution to resolve the scale of the local mean free path. The deterministic nature of the DUGKS also makes it much more efficient than the DSMC for the thermally induced non-equilibrium flows which are featured as very low-speed in nature. The numerical results also show that the thermally induced velocity fields obtained by the Shakhov model in the transition regime exhibit clear differences with the DSMC solutions using the VHS molecular interaction model.

Acknowledgments

The present study is supported by the National Key Research Project (No. 2016YFB0600805) and the National Natural Science Foundation of China (No. 51125024). The authors thank Dr. R.J. Wang for providing us the DSMC data for the micro beam flow case and also her helpful discussions.

References

[1] Y. Sone, Kinetic theory and fluid dynamics, Springer Science & Business Media, LLC, New York, 2002.

[2] A. Ketsdever, N. Gimelshein, S. Gimelshein, N. Selden, Radiometric phenomena: From the 19th to the 21st century, Vacuum 86 (11) (2012) 1644–1662. doi:10.1016/j.vacuum.2012.02.006.

[3] T. Zhu, W. Ye, Origin of Knudsen forces on heated microbeams, Physical Review E 82 (3) (2010) 036308. doi:10.1103/PhysRevE.82.036308.

[4] N. K. Gupta, Y. B. Gianchandani, Thermal transpiration in zeolites: A mechanism for motionless gas pumps, Applied Physics Letters 93 (19) (2008) 193511. doi:10.1063/1.3025304.

[5] D. Jones, Daedalus: Crookes flies high, Nature 392 (6674) (1998) 337–337. doi:10.1038/32784.

[6] D. A. Lockerby, J. M. Reese, M. A. Gallis, The usefulness of higher-order constitutive relations for describing the Knudsen layer, Physics of Fluids 17 (10) (2005) 100609. doi:10.1063/1.1897005.

[7] J. H. Park, S. W. Baek, S. J. Kang, M. J. Yu, Analysis of thermal slip in oscillating rarefied flow using DSMC, Numerical Heat Transfer: Part A: Applications 42 (6) (2002) 647–659. doi:10.1080/10407780290059747.

[8] Z.-H. Li, H.-X. Zhang, Study on gas kinetic unified algorithm for flows from rarefied transition to continuum, Journal of Computational Physics 193 (2) (2004) 708–738. doi:10.1016/j.jcp.2003.08.022.

[9] A. A. Alexeenko, S. F. Gimelshein, E. P. Muntz, A. D. Ketsdever, Kinetic modeling of temperature driven flows in short microchannels, International Journal of Thermal Sciences 45 (11) (2006) 1045–1051. doi:10.1016/j.ijthermalsci.2006.01.014.

[10] M. A. Gallis, J. R. Torczynski, D. J. Rader, M. Tij, A. Santos, Normal solutions of the Boltzmann equation for highly nonequilibrium Fourier flow and couette flow, Physics of Fluids 18 (1) (2006) 017104. doi:10.1063/1.2166449.

[11] K. Aoki, P. Degond, L. Mieussens, Numerical simulations of rarefied gases in curved channels: Thermal creep, circulating flow, and pumping effect, Communications in Computational Physics 6 (5) (2009) 919–954. doi:10.4208/cicp.2009.v6.p919.

[12] J. Nabeth, S. Chigullapalli, A. Alexeenko, Quantifying the Knudsen force on heated microbeams: A compact model and direct comparison with measurements, Physical Review E 83 (6) (2011) 066306. doi:10.1103/PhysRevE.83.066306.

[13] N. Selden, C. Ngalande, N. Gimelshein, S. Gimelshein, A. Ketsdever, Origins of radiometric forces on a circular vane with a temperature gradient, Journal of Fluid Mechanics 634 (2009) 419–431. doi:10.1017/S0022112009007976.

[14] R. W. Bosworth, A. L. Ventura, D. Ketsdever, S. F. Gimelshein, Measurement of negative thermophoretic force, Journal of Fluid Mechanics 805 (2016) 207–221. doi:10.1017/jfm.2016.464.

[15] J. Meng, Y. Zhang, N. G. Hadjiconstantinou, G. A. Radtke, X. Shan, Lattice ellipsoidal statistical BGK model for thermal non-equilibrium flows, Journal of Fluid Mechanics 718 (2013) 347–370. doi:10.1017/jfm.2012.616.

[16] A. D. Strongrich, W. J. O'Neill, A. G. Cofer, A. A. Alexeenko, Experimental measurements and numerical simulations of the Knudsen force on a non-uniformly heated beam, Vacuum 109 (2014) 405–416. doi:10.1016/j.vacuum.2014.05.021.

[17] Z.-H. Li, A.-P. Peng, H.-X. Zhang, J.-Y. Yang, Rarefied gas flow simulations using high-order gas-kinetic unified algorithms for Boltzmann model equations, Progress in Aerospace Sciences 74 (2015) 81–113. doi:10.1016/j.paerosci.2014.12.002.

[18] A.-P. Peng, Z.-H. Li, J.-L. Wu, X.-Y. Jiang, Implicit gas-kinetic unified algorithm based on multi-block docking grid for multi-body reentry flows covering all flow regimes, Journal of Computational Physics 327 (2016) 919–942. doi:10.1016/j.jcp.2016.09.050.

[19] J. Fan, C. Shen, Statistical simulation of low-speed rarefied gas flows, Journal of Computational Physics 167 (2) (2001) 393–412. doi:10.1006/jcph.2000.6681.

[20] N. D. Masters, W. Ye, Octant flux splitting information preservation DSMC method for thermally driven flows, Journal of Computational Physics 226 (2) (2007) 2044–2062. doi:10.1016/j.jcp.2007.06.027.

[21] L. L. Baker, N. G. Hadjiconstantinou, Variance reduction for Monte Carlo solutions of the Boltzmann equation, Physics of Fluids 17 (5) (2005) 051703. doi:10.1063/1.1899210.

[22] K. Xu, Direct Modeling for Computational Fluid Dynamics: Construction and Application of Unified Gas-Kinetic Schemes, Advances in Computational Fluid Dynamics, World Scientific Publishing, 2015. doi:10.1142/9324.

[23] M. Bennoune, M. Lemou, L. Mieussens, Uniformly stable numerical schemes for the Boltzmann equation preserving the compressible Navier-Stokes asymptotics, Journal of Computational Physics 227 (8) (2008) 3781–3803. doi:10.1016/j.jcp.2007.11.032.

[24] F. Filbet, S. Jin, A class of asymptotic-preserving schemes for kinetic equations and related problems with stiff sources, Journal of Computational Physics 229 (20) (2010) 7625–7648. doi:10.1016/j.jcp.2010.06.017.

[25] K. Xu, J.-C. Huang, A unified gas-kinetic scheme for continuum and rarefied flows, Journal of Computational Physics 229 (20) (2010) 7747–7764. doi:10.1016/j.jcp.2010.06.032.

[26] G. Dimarco, L. Pareschi, Asymptotic preserving implicit-explicit Runge-Kutta methods for nonlinear kinetic equations, SIAM Journal on Numerical Analysis 51 (2) (2013) 1064–1087. doi:10.1137/12087606X.

[27] Z. Guo, K. Xu, R. Wang, Discrete unified gas kinetic scheme for all Knudsen number flows: Low-speed isothermal case, Physical Review E 88 (3) (2013) 033305. doi:10.1103/PhysRevE.88.033305.

[28] Z. Guo, R. Wang, K. Xu, Discrete unified gas kinetic scheme for all Knudsen number flows. II. thermal compressible case, Physical Review E 91 (3) (2015) 033313. doi:10.1103/PhysRevE.91.033313.

[29] L. Zhu, Z. Guo, K. Xu, Discrete unified gas kinetic scheme on unstructured meshes, Computers & Fluids 127 (2016) 211–225. doi:10.1016/j.compfluid.2016.01.006.

[30] P. Wang, L. Zhu, Z. Guo, K. Xu, A comparative study of LBE and DUGKS methods for nearly incompressible flows, Communications in Computational Physics 120 (2015) 70–81. doi:10.4208/cicp.240614.171014a.

[31] P. Wang, S. Tao, Z. L. Guo, A coupled discrete unified gas-kinetic scheme for Boussinesq flows, Computers & Fluids 120 (2015) 70–81. doi:10.1016/j.compfluid.2015.07.012.

[32] L. Zhu, P. Wang, Z. Guo, Performance evaluation of the general characteristics based off-lattice Boltzmann scheme and DUGKS for low speed continuum flows, Journal of Computational Physics 333 (2017) 227–246. doi:10.1016/j.jcp.2016.11.051.

[33] E. M. Shakhov, Generalization of the Krook kinetic relaxation equation, Fluid Dynamics 3 (5) (1968) 95–96. doi:10.1007/BF01029546.

[34] L. H. Holway Jr, New statistical models for kinetic theory: methods of construction, Physics of Fluids (1958-1988) 9 (9) (1966) 1658–1673. doi:10.1063/1.1761920.

[35] S. Chen, K. Xu, Q. Cai, A comparison and unification of ellipsoidal statistical and shakhov bgk models, Advances in Applied Mathematics and Mechanics 7 (2) (2015) 245–266. doi:10.4208/aamm.2014.m559.

[36] I. A. Graur, A. P. Polikarpov, Comparison of different kinetic models for the heat transfer problem, Heat and Mass Transfer 46 (2) (2009) 237–244. doi:10.1007/s00231-009-0558-x.

[37] Z.-H. Li, A.-P. Peng, H.-X. Zhang, X.-G. Deng, Numerical study on the gas-kinetic high-order schemes for solving Boltzmann model equation, Science China Physics, Mechanics and Astronomy 54 (9) (2011) 1687. doi:10.1007/s11433-011-4440-8.

[38] L. Wu, J. M. Reese, Y. Zhang, Solving the Boltzmann equation deterministically by the fast spectral method: application to gas microflows, Journal of Fluid Mechanics 746 (2014) 53–84. doi:10.1017/jfm.2014.79.

[39] Z.-H. Li, H.-X. Zhang, Gas-kinetic numerical studies of three-dimensional complex flows on space-craft re-entry, Journal of Computational Physics 228 (4) (2009) 1116–1138. doi:10.1016/j.jcp.2008.10.013.

[40] L. Mieussens, Discrete-velocity models and numerical schemes for the Boltzmann-BGK equation in plane and axisymmetric geometries, Journal of Computational Physics 162 (2) (2000) 429–466. doi:10.1006/jcph.2000.6548.

[41] V. A. Titarev, Conservative numerical methods for model kinetic equations, Computers & Fluids 36 (9) (2007) 1446–1459. doi:10.1016/j.compfluid.2007.01.009.

[42] T. Ohwada, On the construction of kinetic schemes, Journal of Computational Physics 177 (1) (2002) 156–175. doi:10.1006/jcph.2002.7008.

[43] S. Chen, K. Xu, A comparative study of an asymptotic preserving scheme and unified gas-kinetic scheme in continuum flow limit, Journal of Computational Physics 288 (0) (2015) 52–65. doi:10.1016/j.jcp.2015.02.014.

[44] P. Wang, M.-T. Ho, L. Wu, Z. Guo, Y. Zhang, A comparative study of discrete velocity methods for rarefied gas flowsarXiv:1612.06590v1.

[45] Z. Li, M. Fang, X. Jiang, J. Wu, Convergence proof of the DSMC method and the gas-kinetic unified algorithm for the Boltzmann equation, Science China Physics, Mechanics and Astronomy 56 (2) (2013) 404–417. doi:10.1007/s11433-013-4999-3.

[46] G. A. Bird, Molecular Gas Dynamics and the Direct Simulation of Gas Flows, Clarendon Press, 1994.

[47] L. Zhu, S. Chen, Z. Guo, dugksFoam: An open source OpenFOAM solver for the Boltzmann model equation, Computer Physics Communications 213 (2017) 155–164. doi:10.1016/j.cpc.2016.11.010.

[48] T. J. Scanlon, E. Roohi, C. White, M. Darbandi, J. M. Reese, An open source, parallel DSMC code for rarefied gas flows in arbitrary geometries, Computers & Fluids 39 (10) (2010) 2078–2089. doi:10.1016/j.compfluid.2010.07.014.

[49] Y. Sone, Molecular Gas Dynamics: Theory, Techniques, and Applications, 2007. doi:10.1007/978-0-8176-4573-1.

[50] J.-C. Huang, K. Xu, P. Yu, A unified gas-kinetic scheme for continuum and rarefied flows III: Microflow simulations, Communications in Computational Physics 14 (5) (2013) 1147–1173. doi:10.4208/cicp.190912.080213a.

[51] M. Vargas, G. Tatsios, D. Valougeorgis, S. Stefanov, Rarefied gas flow in a rectangular enclosure induced by non-isothermal walls, Physics of Fluids (1994-present) 26 (5) (2014) 057101. doi:10.1063/1.4875235.

[52] A. Passian, A. Wig, F. Meriaudeau, T. L. Ferrell, T. Thundat, Knudsen forces on microcantilevers, Journal of Applied Physics 92 (10) (2002) 6326–6333. doi:10.1063/1.1515108.

[53] A. Passian, R. Warmack, T. L. Ferrell, T. Thundat, Thermal transpiration at the microscale: A Crookes cantilever, Physical Review Letters 90 (12) (2003) 124503. doi:10.1103/PhysRevLett.90.124503.

[54] B. Gotsmann, U. Dürig, Experimental observation of attractive and repulsive thermal forces on microcantilevers, Applied Physics Letters 87 (19) (2005) 194102. doi:10.1063/1.2128040.

[55] N. Selden, C. Ngalande, S. Gimelshein, E. Muntz, A. Alexeenko, A. Ketsdever, Area and edge effects in radiometric forces, Physical Review E 79 (4) (2009) 041201. doi:10.1103/PhysRevE.79.041201.

[56] K. Aoki, S. Takata, H. Aikawa, F. Golse, A rarefied gas flow caused by a discontinuous wall temperature, Physics of Fluids 13 (9) (2001) 2645–2661. doi:10.1063/1.1389283.

[57] W. Su, A. A. Alexeenko, G. Cai, A parallel Runge-Kutta discontinuous Galerkin solver for rarefied gas flows based on 2D Boltzmann kinetic equations, Computers & Fluids 109 (2015) 123–136. doi:10.1016/j.compfluid.2014.12.015.

[58] T. L. Bergman, A. S. Lavine, F. P. Incropera, D. P. DeWitt, Fundamentals of heat and mass transfer, 7th Edition, John Wiley & Sons, 2007.